Electron microscopy of ultra-thin buried layers in InP and InGaAs

By N. GRIGORIEFF and D. CHERNS

H. H. Wills Physics Laboratory, University of Bristol, Tyndall Avenue, Bristol BS8 1TL, UK

M. J. YATES, M. HOCKLY, S. D. PERRIN and M. R. AYLETT

BT Laboratories, Martlesham Heath, Ipswich IP5 7RE, UK

ABSTRACT

The large-angle convergent-beam electron diffraction (LACBED) technique has been used to measure layer thicknesses and strain of ultra-thin arsenic and phosphorus-rich layers produced by temporary arsine and phosphine purges in the metal–organic vapour phase epitaxy growth of InP and InGaAs. The paper describes how the technique, previously used to investigate single quantum wells of thickness between 8 and 30 Å, has been extended to layers of thicknesses of one to two monolayers. It is shown that LACBED patterns can be recorded under conditions in which only a small constant inelastic background and elastic scattering need be considered and can be analysed in detail using a kinematical approach. By combining LACBED results with dark-field images showing the presence of interfacial steps and high-resolution images from cross-sectional samples, a more detailed understanding of the growth interrupt layers is derived.

§ 1. INTRODUCTION

Large-angle convergent-beam electron diffraction (LACBED) has become an established technique for profiling composition and strain in multilayer structures. The LACBED technique generates large-angle rocking curves for a chosen reflection. The technique is closely related to the X-ray rocking curve method which has been extensively applied to profiling semiconductor multilayers (e.g. Fewster (1988)) but differs in the much higher spatial resolution attainable (300 Å in our case, see § 2). The LACBED or 'electron rocking curve' technique has been used to examine semi-conductor multiple quantum well (MQW) and single quantum well (SQW) structures (see Cherns (1989, 1991) and Cherns and Preston (1989) for recent reviews). For SQW structures, Cherns, Jordan and Vincent (1988 a) showed that a 30 Å quantum well of GaAs in nearly 5000 Å of $Al_{0.3}Ga_{0.7}As$, seen in plan-view approximately along the [001] growth direction, gave 200 rocking curves that were sensitive to the GaAs layer. Jordan and others in a number of papers (Jordan, Cherns, Hockly and Spurdens 1989, Jordan *et al.* 1991b) extended the LACBED technique to $InP/In_{0.53}Ga_{0.47}As$ SQW structures. This work, which concentrated on $In_{0.53}Ga_{0.47}As$ quantum wells of thicknesses in the range of 20–100 Å, showed that 200 rocking curves could be used to measure the local quantum well thickness to a sensitivity of one monolayer. Moreover by combining the diffraction information with complementary dark-field images, single atomic steps and small pits in the quantum well were identified.

The sensitivity of 200 rocking curves to the quantum wells in AlGaAs/GaAs and $InP/In_{0.53}Ga_{0.47}As$ depends on the differences in the structure factors between the

quantum well and barrier layers. However, LACBED studies of strained layer structures have shown that rocking curves for diffracting planes inclined to the growth direction are also highly sensitive to layer strains. This depends on the relative rotation of the diffracting planes in oppositely strained layers (Cherns, Kiely and Preston 1988b). Indeed studies of Si/SiGe superlattices (Cherns, Touaitia, Preston, Roussouw and Houghton 1991b) have shown that layer strains as low as $2 \times 10^{-2}\%$ are detectable.

The high sensitivity of electron rocking curves to layer strains is an important factor in the detection and analysis of layers thinner than about 20 Å. For example, layers of InGaAs down to 8 Å thick have been observed in $InP/In_{0.53}Ga_{0.47}As/InP$ films where residual strains $\leqslant 0.1\%$ were present (Cherns 1991). In this paper we show that the LACBED technique can be extended to study layers only one or two monolayers thick where much larger layer strains are involved. The samples described here contain thin InAsP layers in InP and thin InGaAsP layers in $In_{0.53}Ga_{0.47}As$ produced by short growth interrupts in metal–organic vapour phase epitaxy (MOVPE) which were studied to elucidate the effects of gas switching at interfaces in MOVPE. In §2 the application of LACBED to the investigation of ultra-thin layers is explained and discussed. It is then shown that LACBED can be used to measure the local thickness of the growth interrupt layers. Furthermore dark-field imaging is used to identify the presence of individual atomic steps in these layers. It is shown that the topology and average thickness of the InAsP layers in InP and InGaAsP layers in $In_{0.53}Ga_{0.47}As$ are quite different throwing new light on the MOVPE growth mechanism.

§2. THE LACBED METHOD

It is useful to outline briefly first the method by which LACBED patterns are obtained and the information contained therein. Figure 1 shows schematically how a LACBED pattern is generated. A convergent electron beam is focused either below (as shown) or above the specimen such that in the image plane the focused spots due to the straight-through and diffracted beams are well separated. A selected-area aperture can be used to select one spot to give a single disc in the corresponding diffraction pattern.

The LACBED pattern has several advantages over conventional CBED patterns.

(1) The limitation on convergence angle in CBED due to beam overlap is absent in LACBED so that very large convergence angles are possible in microscopes with condenser/objective lenses; in our experiments using a Philips EM 430 in nanoprobe mode, a convergence angle of 6° is routinely used.

(2) Diffracted beams from different parts of the illuminated region of the specimen contribute to different parts of the diffraction disc. The diffraction disc, therefore, has spatial information, the spatial resolution being given approximately by the minimum probe size (Vincent 1989). In our work resolution was not an important factor and a large spot size of about 300 Å was chosen to give high intensity in the diffraction disc. The resolution is also limited by the semi-angle α (see fig. 1) giving a limit of about 30 Å for the settings given in §3 which is much smaller than the probe size used and hence did not limit the actual resolution.

(3) The selected-area aperture acts like an objective aperture in imaging mode to filter-out inelastic background. Since the angular acceptance can be very small (down to 1 mrad in our case) LACBED patterns can contain useful information out to very large values of the deviation parameter s. The need for such filtering is discussed further below.

Fig. 1
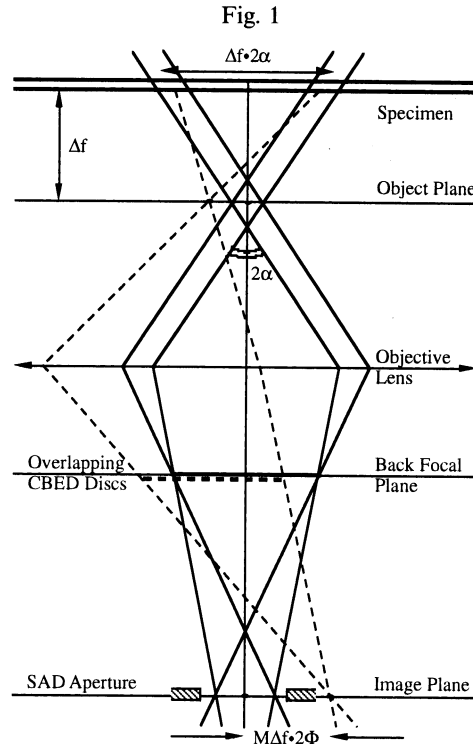
Ray diagram excluding aberration, for a specimen illuminated by a defocused beam with finite diameter in the object plane. Dashed lines indicate a diffracted beam. α is the semi-acceptance angle of the SAD aperture, Δf the defocus, M the objective demagnification and Φ the Bragg angle.

An example of a LACBED pattern from an $InP/In_{0.53}Ga_{0.47}As$ SQW structure is shown in fig. 2. The improvement in diffraction detail (and angle) compared with the corresponding conventional CBED pattern can be seen. The LACBED pattern in fig. 2 shows the variation in diffraction intensity in the 200 reflection as a function of the deviation parameter s. Assuming that the specimen is parallel-sided and flat, i.e. ignoring spatial variation for the moment, the LACBED pattern constitutes an electron rocking curve for the 200 reflection.

2.1. Analysis of electron rocking curves

The rocking curves obtained by the method described above need to be analysed to deduce the crystal structure. This is done by digitizing LACBED patterns and by subsequent curve fitting on a computer. The procedure adopted here (§ 3) requires the simulation of typically 10^4 rocking curves for each experimental result. An accurate simulation of such rocking curves for all values of s requires the dynamical theory of diffraction (e.g. Hirsch, Howie, Nicholson, Pashley and Whelan (1965)). However the computing power involved is relatively large and a curve fitting process based on the dynamical theory is not feasible. The kinematical theory of diffraction offers a practical alternative although it breaks down in the case of strong diffraction, i.e. for small deviation s, from the Bragg position. A comparison of kinematical and dynamical

Fig. 2

$\overline{400}$ $\overline{200}$ 000 200 400

-0.01   0   0.01

s (Å⁻¹)

(a)   (b)
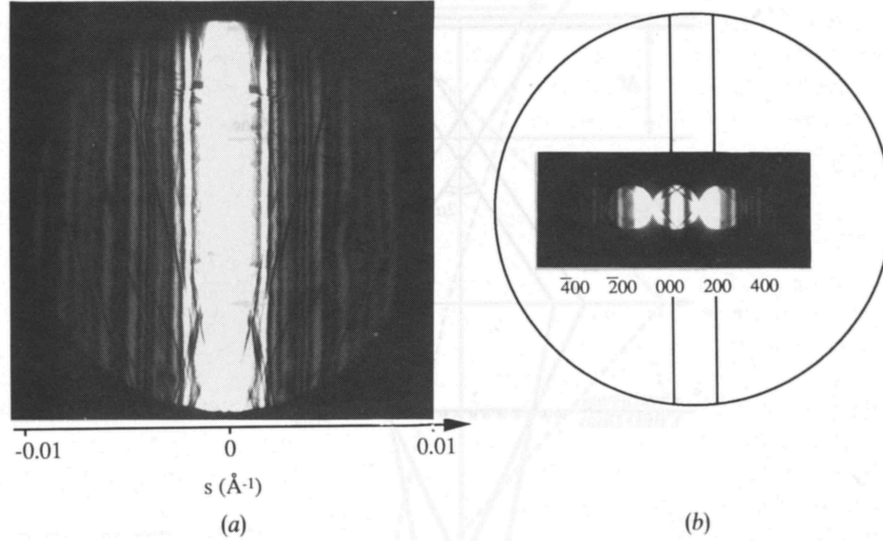
(a) 200 LACBED pattern from a 32 Å In$_{0.53}$Ga$_{0.47}$As well clad between 1500 Å of InP. The modulation of the fringe intensity is clearly visible. In (b) a conventional CBED pattern is displayed showing the difference in angle and background intensity between LACBED and CBED.

rocking curves for the experiments described here showed that kinematical theory gave a good approximation for s larger than approximately 0·004 Å⁻¹. In the analyses of §5 comparisons of theory and experiment have been carried out for $|s| > 0·004$ Å⁻¹.

If $\mathbf{k}$ and $\mathbf{k}'$ are the wave-vectors of the incident and the diffracted beam one can define a diffraction vector $\mathbf{K} = \mathbf{k}' - \mathbf{k}$. By introducing the reciprocal lattice one can rewrite $\mathbf{K} = \mathbf{g} + \mathbf{s}$ where $\mathbf{g}$ is a reciprocal lattice vector and the deviation parameter $\mathbf{s}$ is parallel to the crystal surface normal $\mathbf{n}$ and positive in the direction of the beam. The kinematical amplitude $\Phi(\mathbf{K})$ of the diffracted beam for unit incident intensity is then given by

$$\Phi(\mathbf{K}) = \frac{1}{V_c} \int_0^T F(\mathbf{K}, z) \exp\{-2\pi i[sz + \mathbf{g} \cdot \mathbf{R}(z)]\} \, dz, \tag{1}$$

where z is the distance from the crystal surface along the surface normal, T the crystal thickness, V_c the volume of the unit cell and $\mathbf{R}(z)$ the displacement of the unit cell due to strain. The scattering from one unit cell is given by

$$F(\mathbf{K}, z) = \sum_i f_i(\mathbf{K}, z) \exp[-2\pi i \mathbf{K} \cdot \mathbf{r}_i(z)], \tag{2}$$

where $\mathbf{r}_i$ is the position of the ith atom within the unit cell and $f_i(\mathbf{K}, z)$ the atomic scattering factor for electrons. If $\mathbf{s} = 0$ then $\mathbf{K} = \mathbf{g}$ and F is equal to the structure factor F_g normally used to describe scattering from a unit cell. Equation (1) resembles the Fourier transform of $F(\mathbf{K}, z)$ along the z axis and leads to a rocking curve with a fringe spacing in the reciprocal space of

$$\Delta s = 1/T. \tag{3}$$

The specimens examined all contain a buried, thin layer whose composition and strain differ from the surrounding (cladding) layers. The typical thickness of the cladding layers is about 2000 Å in total. For this tricrystal structure the validity of eqn. (1) needs to be examined in the case where the thickness of the buried layer approaches atomic dimensions. For crystals with buried layer thicknesses 8 Å and more eqn. (1) gave good results. For buried layers of subunit cell thickness scattering from individual layers has to be considered. $\Phi(\mathbf{K})$ is then given as

$$\Phi(\mathbf{K}) = \frac{1}{A_c} \sum_j F_j(\mathbf{K}) \exp(-2\pi i \mathbf{K} \cdot \mathbf{r}_j) \tag{4}$$

where $\mathbf{r}_j$ designates the position of the jth unit cell within the crystal and the sum over j is to be taken over one string of unit cells through the crystal along $\mathbf{c}$, the lattice vector with a component into the crystal. The lattice vectors $\mathbf{a}$ and $\mathbf{b}$ are assumed perpendicular to $\mathbf{n}$ (if this is not the case, it is possible in all practical cases to redefine the unit cell accordingly), $A_c = |\mathbf{a} \times \mathbf{b}|$ and $F_j(\mathbf{K}) = F(\mathbf{K}, z)$ if z equals the distance of the jth layer from the surface. Strain and rigid shifts at interfaces can be easily dealt with by changing the position vectors $\mathbf{r}_i$ of the individual atoms (see eqn. (2)) as well as the coordinates of the unit cells $\mathbf{r}_j$ (see eqn. (4)) by $\Delta\mathbf{r}_i$ and $\Delta\mathbf{r}_j$. The samples described in this paper have an f.c.c. lattice and $\mathbf{c}$ coincidences with the growth direction [001]. A buried layer with a lattice parameter different from the cladding layers will result in strain along the growth direction [001] and $\Delta\mathbf{r}_i$ and $\Delta\mathbf{r}_j$ will be parallel to $\mathbf{c}$ and [001]. This means a rotation of planes inclined to [001] and reflections (e.g. 202) coming from these planes are sensitive to layer strain. To take account of monolayers (i.e. incomplete unit cells) a new unit cell has to be defined which will only contain the atoms corresponding to one monolayer. With this fractioned cell comes an additional translation of the following layers to match the interface of the incomplete layer. In the case of a f.c.c. lattice with an incomplete (001) layer the translation vector is either $\mathbf{R} = (0{\cdot}5, 0, 0{\cdot}5)$ or $\mathbf{R} = (0, 0{\cdot}5, 0{\cdot}5)$. This means that for any allowed reflection g_{hkl} where hkl are all even or all odd, the dot product $\mathbf{g} \cdot \mathbf{R} =$ integer which can be neglected in the exponential.

§3. Background in rocking curves

The analysis of rocking curves involves measurement of intensity ratios of adjacent maxima. Therefore it is important to identify the background intensity in those maxima to remove it and calculate the true ratios. As noted earlier the selected area diffraction (SAD) aperture functions as a very effective angular filter for inelastically scattered electrons, which makes it possible to observe even weak contrast normally invisible in conventional convergent beam patterns (Jordan, Rossouw and Vincent, 1991a). Inelastic background due to thermal diffuse scattering (TDS) and plasmon losses are characterized by angular distributions $d\lambda_{TDS}^{-1}/d\Omega$ and $d\lambda_p^{-1}/d\Omega$, λ_{TDS} and λ_p being the mean free paths for TDS and plasmon scattering and Ω the solid angle. This leads to cones of inelastically scattered electrons about each ray passing through the specimen. Excluding a large fraction of those electrons with the SAD aperture means an increase in the effective mean free paths by several orders of magnitude. For plasmon scattering this can be measured by electron energy loss spectroscopy (EELS) (Jordan *et al.* 1991a). However the remaining background intensity can falsify the true fringe intensity of a rocking curve and subsequently introduce an error in its analysis. The inelastic intensity is proportional to the elastic component and will be convoluted with the elastic intensity in angular space. All rays associated with a particular reflection come

to focus in the image plane and the SAD aperture will truncate each inelastic cone to a maximum semiangle α. The defocus Δf, the demagnification M of the SAD aperture at the specimen and SAD aperture diameter D are related to semiangle α by

$$\alpha = \frac{D}{2\Delta f M}.$$ (5)

Assuming an ideal optical system, i.e. neglecting aberrations and astigmatism, this model leads to a two-dimensional top hat function with angular half-width α and a height corresponding to the inelastic fraction of intensity, convoluted with the elastic signal. It follows that the intensity at each point on an experimental rocking curve includes an inelastic term equal to the inelastic intensity integrated over the angular half-width α. If α is smaller than half the angular separation of the fringes in the rocking curve, the inelastic term in a particular fringe peak will only include contributions from an area including the same fringe and will therefore be proportional to the elastic term, and the measured total will give the true relative elastic peak intensity to be used for further analysis (§ 5). For a sample of total thickness T and a reflection **g** the angular separation of adjacent fringes will be

$$\Delta\alpha = \frac{1}{T|\mathbf{g}|},$$ (6)

using the kinematical result, eqn. (3), which translates to a defocus of

$$\Delta f = \frac{DT|\mathbf{g}|}{M}.$$ (7)

Thus for $M = 40$, $D = 2\,\mu\text{m}$, $\mathbf{g} = 200$ in InP ($a = 5.869\,\text{Å}$) and $T = 2000\,\text{Å}$, $\Delta f = 34\,\mu\text{m}$.

Additional background intensity comes from other reflections including the transmitted beam. Each will be accompanied by a halo of inelastically scattered electrons extending over the SAD aperture. At large defocus this contribution will be small. When the SAD aperture is placed on a first-order reflection, e.g. 200 or 202, the additional background mainly comes from the transmitted beam and will be approximately constant in the range of orientations used. This background depends on the defocus and can be estimated from the minima at the low intensity end (at larger s) of the rocking curve.

In general both the convoluted and the roughly constant background will be present in an experimental rocking curve. However depending on the filtering conditions different assumptions can be made. If the filtering is good enough, i.e. eqn. (7) holds, then it is sufficient to subtract just a constant. If on the other hand the defocus is not large enough to satisfy eqn. (7) the convoluted background will approximately follow an average intensity of the rocking curve, which is proportional to $1/s^2$. The local

Table.   Samples examined and buried layer thicknesses measured by LACBED assuming 100% group V substitution in the thin layers. One monolayer $= 2.9\,\text{Å}$.

Sample	InP/InAs/InP		InGaAs/InGaP/InGaAs	
Purge in seconds	5	50	5	25
Measured layer thickness in monolayers	1.1 ± 0.2	1.6 ± 0.2	1.2 ± 0.2	1.7 ± 0.2

background can then be estimated from the minima between the maxima and subtracting a monotonically decreasing function following the minima will both remove the constant and convoluted background.

Since the experimental relative intensities can be measured fairly accurately the error in the measured buried layer thickness (i.e. about one-fifth of a monolayer, see the table) will be due mainly to the error in the background estimate.

§ 4. Experimental

Tricrystals of InGaAs/InGaAsP/InGaAs and InP/InAsP/InP were isolated from the structure shown in fig. 3 using selective etches giving samples with a thin area of typically 1 mm^2. The structures were grown on [001] InP substrates using atmospheric pressure MOVPE. One pair of samples contained thin arsenic-rich layers in InP, the other pair contained phosphorus-rich layers in InGaAs (In/Ga = 0·53/0·47). All four samples were produced by interrupting the growth and purging the reactor with arsine or phosphine according to the times in fig. 3, before normal growth conditions were restored. Phosphorus and arsenic were expected to substitute each other up to a certain depth thus creating thin, strained layers of InAsP in InP and InGaAsP in InGaAs (fig. 3). Rocking curves as well as images were obtained in 200 and 202 reflections. Cross-sections were produced and high resolution images were obtained to confirm the results.

§ 5. Results and interpretation

200 rocking curves were recorded with defocus Δf sufficient to remove the convoluted inelastic background as discussed in § 3. However in order to obtain 202 LACBED discs the samples had to be tilted to 45°, which caused a variation of the sample height within the illuminated area. For larger defocus this led to a broadening of the diffracted beam in the image plane, thus limiting the maximum possible defocus to about 30 μm (to achieve conditions described in § 3, 48 μm would be necessary). Rocking curves for 200 and 202 reflections are illustrated in fig. 7.

Fig. 3

(a)
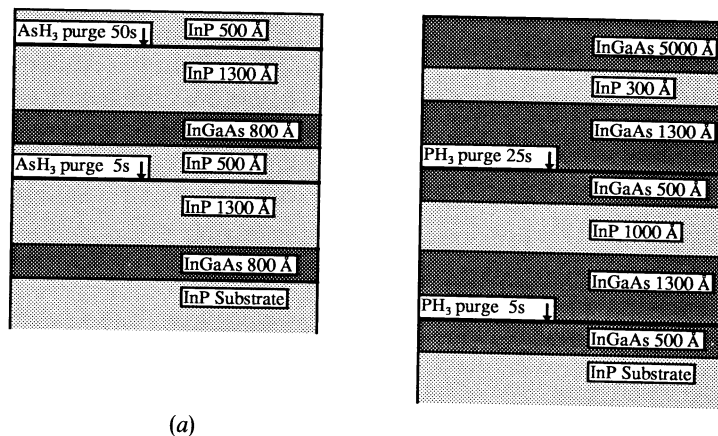
Schematic cross-sections of the samples prior chemical etching. (a) shows the InP samples exposed to arsine. The InGaAs layers act as an etch stop to allow separation of the tricrystals from the structure. (b) represents the InGaAs samples exposed to phosphine. Here a thin InP layer separating the two tricrystals forms the etch stop.

The rocking curves were digitized on a scanner, model Optronics Photoscan P1000, to give an array of typically 600×600 pixels with a resolution of 256 grey levels proportional to optical density units between 0 and 2. From these arrays a set of maxima and minima was measured by reading about 100 to 200 pixels along each fringe, which gave average intensities and standard deviations for each maximum and minimum. Where possible the scanned area was chosen to exclude perturbations of fringe intensities by non-systematic reflections or by irregularities in the sample. Remaining perturbations were assumed to have only a small effect on the measured average. Before further processing the inelastic background was stripped (see § 3). The sets of maxima and minima were then matched by theoretical curves employing eqn. (4) using a computer. Theoretically, the minima of the rocking curves from the samples were close to zero, i.e. not sensitive to the buried layer. Therefore, only the calculation and comparison of the intensities of the maxima was necessary. Interpreting the sets of N maxima as N-component vectors one can normalize the vectors and take the magnitude of the difference vector as a measure for the degree of fit. This made the process very sensitive to small relative errors in the higher maxima. To avoid this the N-ratios of adjacent maxima were calculated to form $(N$-1)-component vectors used for comparison; thereby the algorithm was stabilized and the sets were normalized at the same time. The ratios were weighted with the standard deviations of the corresponding experimental maxima.

Simulations for 200 reflections which are sensitive to composition but not to layer strains showed that rocking curves depend on the product $t_b x$, x designating the fraction of substituted material in the buried layer (i.e. $InAs_x P_{1-x}$ or $In_{0.53}Ga_{0.47}As_{1-x}P_x$). For 202 reflections the product has to be replaced by $t_b \varepsilon$, where $\varepsilon = (c - c_0)/c_0$ is the strain of the buried layer in the growth direction and c_0 and c are the lattice parameters of the cladding and strained buried layer material parallel to the growth direction. Thus in both cases the layer thickness and composition are interdependent (strain is approximately proportional to composition). This ambiguity is an inherent limit of the LACBED technique: a rocking curve resembles the power spectrum (squared magnitude of the Fourier transform) of $F(\mathbf{K}, z)$ (see § 2.1) and therefore contains detailed information of the buried layer, its interfaces (e.g. grading) and the composition profile in the z direction in the rest of the sample (e.g. compositional tails, see § 5.1). Owing to the limited range of frequencies (i.e. deviation parameter s) in an experimental rocking curve this information is limited to a certain spatial resolution along the z axis. A rocking curve from a tricrystal with a buried layer thickness t_b shows modulation with a sinusoidal amplitude (Jordan *et al.* 1989) whose first minimum lies at a value of $s = 1/t_b$, and rocking curves including this value will allow reconstruction of the composition profile with a resolution of at least t_b. Hence the resolution limit can be taken as

$$\Delta z = 1/s_{max}, \tag{8}$$

where s_{max} is the maximum s recorded. Larger values of s_{max} will increase the resolution although the diffracted intensity normally falls below practical limits. In this work $s_{max} \approx 0.014 \, \text{Å}^{-1}$ and $\Delta z \approx 70 \, \text{Å} \approx 24$ monolayers. In practice Δz can be expected to be better than the limit given by eqn. (8), since the analysis of a rocking curve does not depend on the position of the minimum of the modulation, but the shape of the whole curve which is matched by a curve fitting process (see above). The position of the modulation minimum is not changed by the inelastic background and can always be determined accurately. However, as described in § 3, the curve matching procedure is

sensitive to the inelastic background and the maximum resolution will depend on the uncertainty (noise) in the measured intensity of the fringe peaks. The interdependence of t_b and composition in the case of $t_b \ll \Delta z$ may be understood by investigating eqn. (4). This is shown in the Appendix.
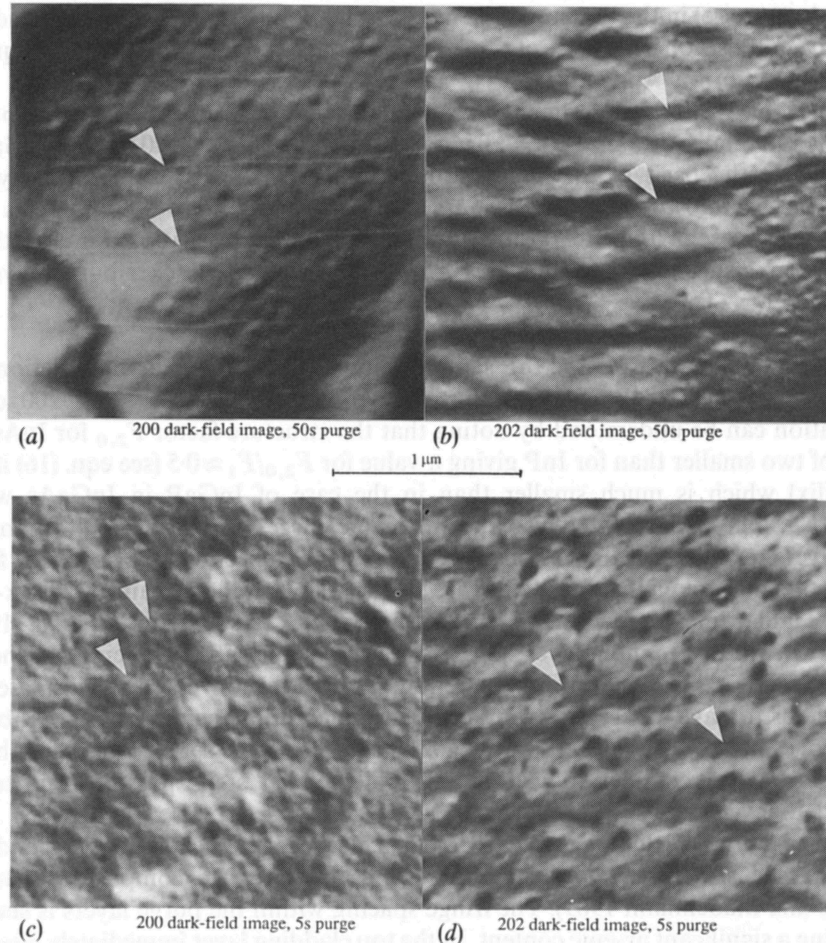
In the table we fit the experimental results assuming 100% substitution in the buried layer such that layer strains are $\varepsilon = 0.034$ for InAs in InP and $\varepsilon = -0.035$ for InGaP in InGaAs. On the basis of this assumption it can be seen that approximately one monolayer was substituted in the 5 s purged samples and about 1·5 monolayers were substituted in case of longer exposure. From the preceding discussion it is clear that if substitution is substantially less than 100% we must assume thicker buried layers.

5.1. *Thin InAs layers in InP*

200 rocking curves from the InP samples showed only very weak modulation and the analysis was based on the strain-sensitive 202 curves. The weak 200 curve modulation can be understood by noting that the structure factor $F_{2,0}$ for InAs is a factor of two smaller than for InP giving a value for $F_{2,0}/F_1 \approx 0.5$ (see eqn. (16) in the Appendix) which is much smaller than in the case of InGaP in InGaAs where $F_{2,0}/F_1 > 4$. The layers created by 5 and 50 s arsine purges were measured to 1 and 1·5 monolayers respectively. Images taken in 200 and 202 reflections are shown in fig. 4. For the 50 s purge equally spaced lines are clearly visible in the 200 and 202 dark-field images. Similar lines were found in earlier studies on SQWs (e.g. Jordan *et al.* (1989)) and were attributed to monolayer steps introduced by the substrate being polished at an off-angle from the exact [001] crystallographic direction. Owing to the mismatch we expect steps to have a varying strain field causing additional step contrast visible as dark fringes parallel to the steps in the 202 image. The same set of images for the 5 s purge shows broken lines indicating less well defined steps possibly due to an incomplete layer.

In fig. 5 a bright-field image ($U = [010]$) of a cleaved cross-section of the 5 and 50 s arsine purged structures shows thickness fringes sensitive to composition (Buffat, Ganiére and Stadelmann 1989). The fringe spacing within the purge layers is smaller indicating a significant arsenic content. In the top cladding layer immediately after the purge the thickness fringes are bent suggesting arsenic tails in InP. The shift of the fringes near the purged layer appear to be larger after the 50 s purge indicating a higher arsenic content. According to the arguments given in § 5 the tails will alter the rocking curve modulation whereby parts of the arsenic content in the tail will be integrated in the buried layer thickness measured by LACBED, depending on the spatial resolution. An estimate of the tail length from fig. 5 gave 100 to 150 Å. High-resolution images from cross-sections of the two arsine purged samples in fig. 6 show layers of thicknesses of one or two monolayers with well defined interfaces. This suggests a thin buried layer with a high arsenic content and a tail starting off with an arsenic concentration well below that of the thin layer. To show the effect of such a tail on the LACBED results a simulated rocking curve of a structure including one monolayer of InAs and a tail with an exponentially decreasing arsenic concentration $c = c_0 \exp(-\lambda z)$ starting with an initial concentration $c_0 = 25\%$ and $\lambda = 1/60$ Å was produced. The total arsenic content of this structure equals 5·1 monolayers. The fringe peaks of this rocking curve were then processed the same way as a set of stripped maxima from an experimental curve (see § 5) admitting only tricrystals with sharp interfaces as trial structures which gave a buried layer equivalent to 2·0 monolayers of InAs. This shows that a tail increases the buried layer thickness measured by LACBED although the increase is much smaller than the

Fig. 4

(a) 200 dark-field image, 50s purge   (b) 202 dark-field image, 50s purge

1 μm

(c) 200 dark-field image, 5s purge   (d) 202 dark-field image, 5s purge

Dark-field images from the InP samples purged with arsine. (a) and (b) show linear contrast (arrows) in the 50 s purge samples due to interfacial steps of monolayer height. The 202 image in (b) has additional contrast around the lines indicating a strain field associated with the steps which is not visible in the 200 image in (a). Images (c) and (d) are the corresponding dark-field images from the 5 s purge sample. The linear contrast is significantly reduced suggesting poorly defined interfacial steps.

total equivalent in monolayers present in the tail. The actual arsenic content in the tails seen in fig. 5 is not known and the results given in the table have to be taken as upper limits for the true buried layer thicknesses.

5.2. Thin InGaP layers in InGaAs

Figure 7 displays experimental and simulated 200 and 202 rocking curves for the InGaAs samples purged with phosphine which reveal a clear difference in modulation between the 5 and 25 s purges. The weak fringes were most affected. The results in the table suggest that substitution of more than one monolayer occurred in the 25 s phosphine purge in InGaAs. Phosphorus tails in InGaAs were not observed in a bright-field image of a cleaved cross-section in fig. 8. Dark-field images in 200 and 202

Fig. 5
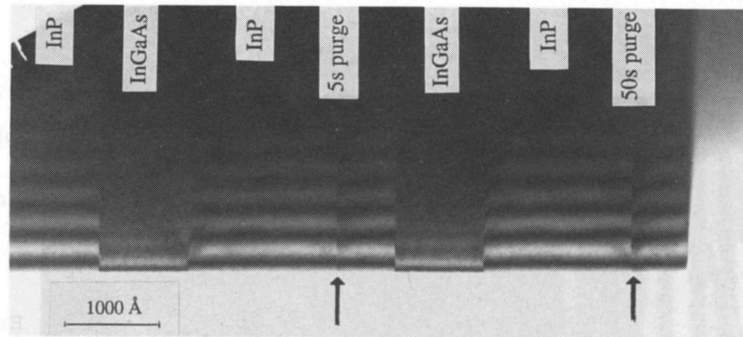
Bright-field image of a cleaved cross-section showing the thin InAsP layers (indicated) in InP (see fig. 3). $U = [010]$. Arsenic tails in the subsequently grown InP layer are observable as bent contours.

Fig. 6

5s AsH₃ purge on InP   50s AsH₃ purge on InP
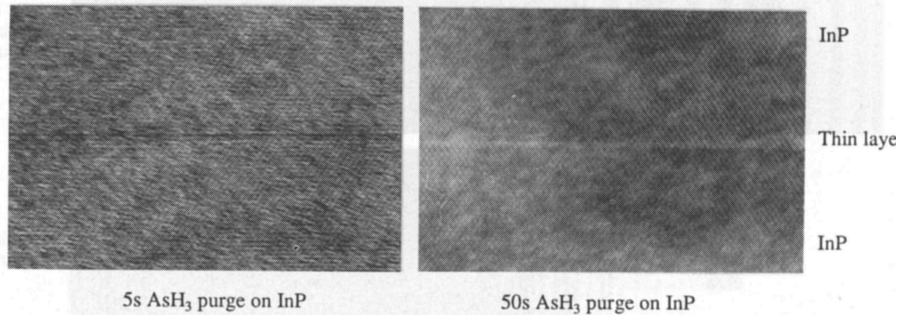
High-resolution images from the InP samples purged with arsine. Both images suggest a thin layer of one or two monolayers thickness with sharp interfaces.

reflections do not reveal the linear features seen in the arsine purge cases. This indicates rough interfaces of the buried layers. High-resolution images from the two phosphine purged samples in fig. 9 verify the results. The interfaces of both buried layers exhibit rough interfaces. The contrast from the 5 s purged sample is significantly reduced compared with the 25 s purged sample indicating a smaller phosphorus content.

§6. CONCLUSIONS

The LACBED technique was shown to be able to measure strained, buried layer thicknesses produced in InP and InGaAs during MOVPE growth interrupts and purges with arsine or phosphine. Assuming 100% substitution in the buried layer it was shown that approximately one or 1·5 monolayers were substituted in InP exposed to arsine and InGaAs exposed to phosphine depending on the time of exposure. In the InP/arsine purged case it was also possible to image interfacial steps of one monolayer height. This was not possible with the InGaAs/phosphine purged sample as the interfaces were rough on a near-atomic scale. High-resolution images of cross-sections were consistent with the diffraction and imaging results.
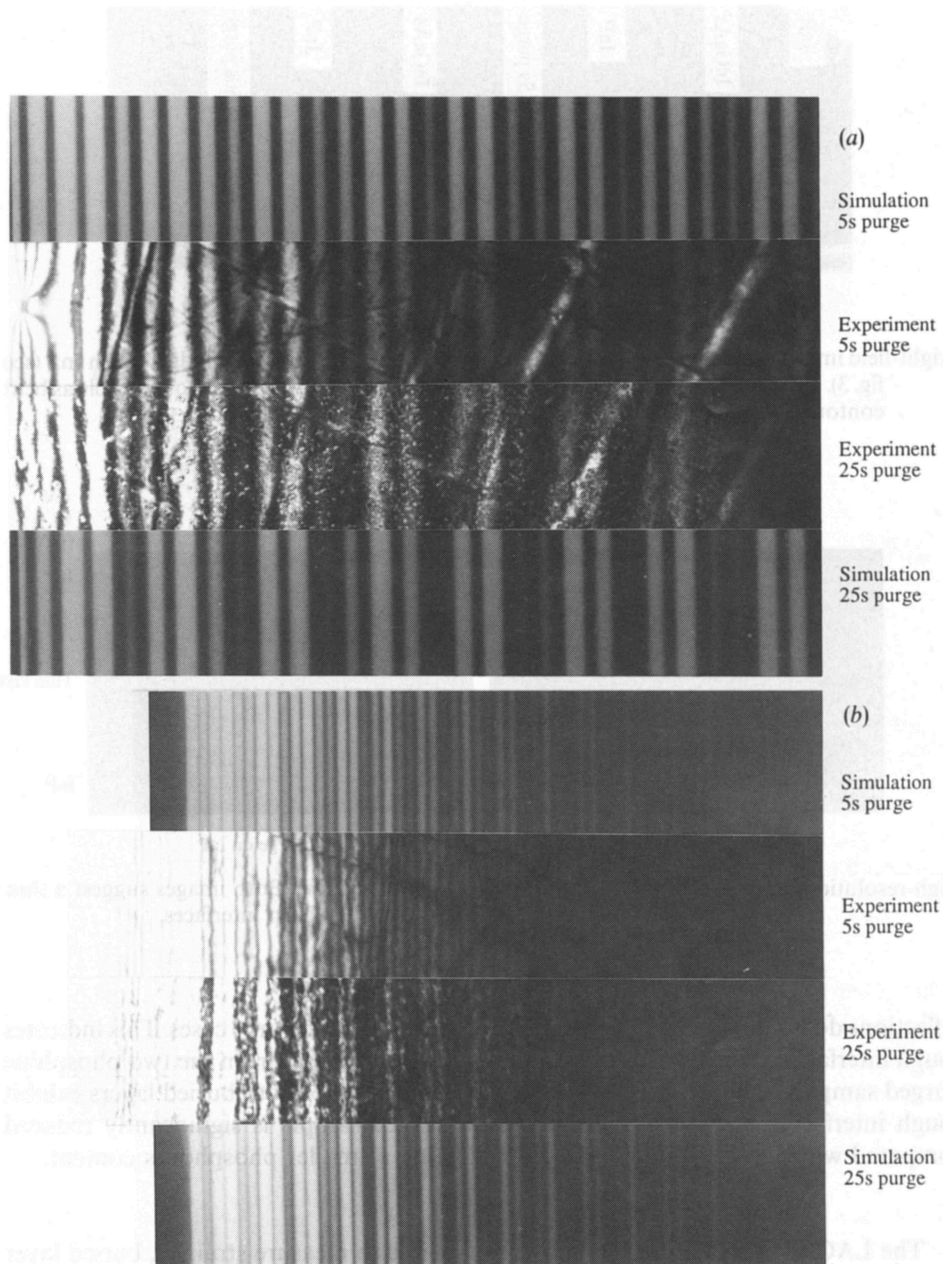
Simulated and experimental 200 and 202 rocking curves from the InGaAs samples exposed to
phosphine. In both reflections the difference in modulation is visible, the modulation
being stronger in the 25 s purge sample indicating a thicker layer. The weak fringes are
most affected.

Fig. 8
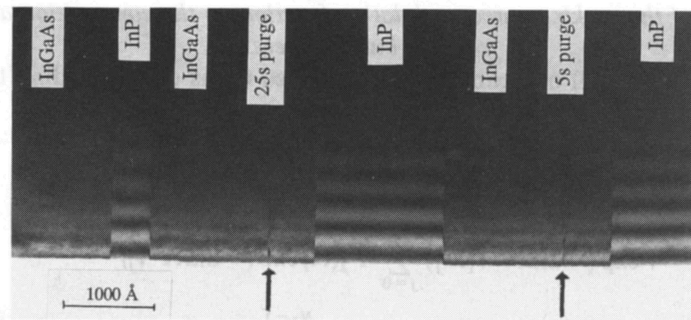
Bright-field image of a cleaved cross-section from the InGaAs sample purged with phosphine (see fig. 3). The buried layers are indicated. $U = [010]$. There is no evidence of a phosphorus tail in the top InGaAs layer.

Fig. 9
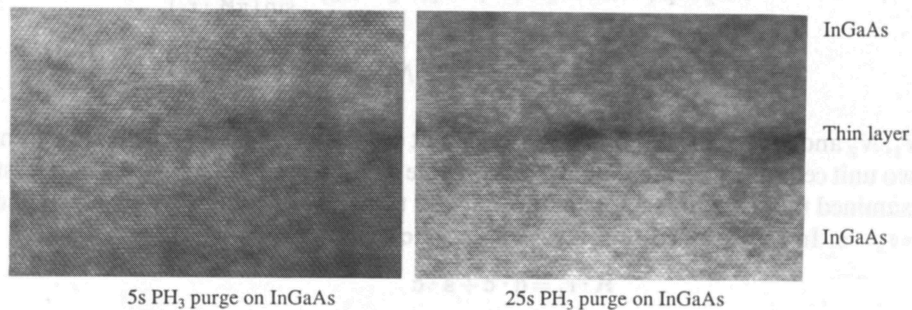
High-resolution images from the InGaAs samples exposed to phosphine. The images suggest rough interfaces in both cases. Stronger contrast is visible in the 25 s purge case indicating a higher phosphorus content.

In the case of the InP samples the results of the cleaved cross-sections (fig. 5) indicate a tail of arsenic into the subsequently grown InP layer, suggesting that some arsine remains in the reactor chamber following the resumption of InP growth. The effect of this additional arsenic is to increase $t_b\varepsilon$ as measured by LACBED (see § 5.1) and thus lead to an overstimate of the degree of substitution in the purge layer itself which has to be considered in the interpretation of the results. In the case of InGaAs exposed to phosphine there is no evidence of a phosphorus tail in this sample (fig. 8). Our results indicate the substitution of at least one monolayer after 5 s and further substitution for longer pauses.

APPENDIX

Dependence of the rocking curve modulation function on the composition and strain of thin buried layers

Employing eqn. (4) one can write down three terms corresponding to the three layers in a tricrystal:

$$\Phi(\mathbf{K}) = \frac{1}{A_c} \left\{ \sum_{j=0}^{N_1-1} F_1(\mathbf{K}) \exp(-2\pi i \mathbf{K} \cdot \mathbf{r}_j) \right.$$

$$+ \exp(-2\pi i \mathbf{K} \cdot \mathbf{r}_1 N_1) \sum_{j=0}^{N_2-1} F_2(\mathbf{K}) \exp(-2\pi i \mathbf{K} \cdot \mathbf{r}_j)$$

$$\left. + \exp[-2\pi i \mathbf{K} \cdot (\mathbf{r}_1 N_1 + \mathbf{r}_2 N_2)] \sum_{j=0}^{N_3-1} F_3(\mathbf{K}) \exp(-2\pi i \mathbf{K} \cdot \mathbf{r}_j) \right\}$$

$$= \frac{1}{A_c} \left\{ F_1 \exp[-\pi i \mathbf{K} \cdot \mathbf{r}_1(N_1-1)] \frac{\sin(\pi \mathbf{K} \cdot \mathbf{r}_1 N_1)}{\sin(\pi \mathbf{K} \cdot \mathbf{r}_1)} \right.$$

$$+ F_2 \exp\{-\pi i \mathbf{K} \cdot [2\mathbf{r}_1 N_1 + \mathbf{r}_2(N_2-1)]\} \frac{\sin(\pi \mathbf{K} \cdot \mathbf{r}_2 N_2)}{\sin(\pi \mathbf{K} \cdot \mathbf{r}_2)}$$

$$\left. + F_3 \exp\{-\pi i \mathbf{K} \cdot [2\mathbf{r}_1 N_1 + 2\mathbf{r}_2 N_2 + \mathbf{r}_3(N_3-1)]\} \frac{\sin(\pi \mathbf{K} \cdot \mathbf{r}_3 N_3)}{\sin(\pi \mathbf{K} \cdot \mathbf{r}_3)} \right\}. \quad (9)$$

N_1, N_2 and N_3 are the layer thicknesses in unit cells and $\mathbf{r}_1$, $\mathbf{r}_2$ and $\mathbf{r}_3$ the vectors joining two unit cells in adjacent monolayers along the column of summation. In the tricrystals examined the structure factors in the first and third layer F_1 and F_3 were equal and $\mathbf{r}_1 = \mathbf{r}_3 = \mathbf{c}$. In the strained thin layer $\mathbf{r}_2 = \mathbf{r}_1 + \varepsilon \mathbf{c}$. It is

$$\mathbf{K} \cdot \mathbf{r}_1 = \mathbf{g} \cdot \mathbf{c} + \mathbf{s} \cdot \mathbf{c}$$

$$= \text{integer} + \mathbf{s} \cdot \mathbf{c}, \quad (10)$$

and

$$\mathbf{K} \cdot \mathbf{r}_2 = \mathbf{g} \cdot \mathbf{c} + \mathbf{s} \cdot \mathbf{c} + \mathbf{g} \cdot \varepsilon \mathbf{c} + \mathbf{s} \cdot \varepsilon \mathbf{c}$$

$$\approx \text{integer} + \mathbf{s} \cdot \mathbf{c} + \mathbf{g} \cdot \varepsilon \mathbf{c}, \quad (11)$$

neglecting the last term in eqn. (11) since $\mathbf{s} \cdot \varepsilon \mathbf{c} \ll \mathbf{s} \cdot \mathbf{c} + \mathbf{g} \cdot \varepsilon \mathbf{c}$. The integer does not change the exponential and the sin-functions and can be neglected. For N_2 and $\mathbf{s}$ small it follows that in the second term in eqn. (9)

$$\frac{\sin(\pi \mathbf{K} \cdot \mathbf{r}_2 N_2)}{\sin(\pi \mathbf{K} \cdot \mathbf{r}_2)} \approx N_2. \quad (12)$$

To see the effect of the thin buried layer it is convenient to write the amplitude $\Phi(\mathbf{K})$ as a sum consisting of a term $\Phi_0(\mathbf{K})$ describing the scattering from a single crystal of thickness $N_0 = N_1 + N_2 + N_3$ and a modulation term $\Delta\Phi(\mathbf{K})$ due to the thin buried layer:

$$\Phi(\mathbf{K}) = \Phi_0(\mathbf{K}) + \Delta\Phi(\mathbf{K}), \quad (13)$$

with

$$\Phi(\mathbf{K}) = \frac{1}{A_c} F_1 \exp[-\pi i \mathbf{K} \cdot \mathbf{r}_1(N_0-1)] \frac{\sin(\pi \mathbf{K} \cdot \mathbf{r}_1 N_0)}{\sin(\pi \mathbf{K} \cdot \mathbf{r}_1)}. \quad (14)$$

In the case of composition sensitive reflections (e.g. 200) $F_1 = F_3 \neq F_2$ and $\mathbf{g} \cdot \varepsilon\mathbf{c} = 0$ and only the second term in eqn. (9) will produce a difference which is readily calculated as

$$\Delta\Phi(\mathbf{K}) = \frac{F_1}{A_c}\left(\frac{F_2}{F_1} - 1\right)\exp\left[-\pi i\mathbf{s} \cdot \mathbf{c}(2N_1 + N_2 - 1)\right]N_2. \tag{15}$$

F_2 changes with composition x as $F_2 = xF_{2,0} + (1 - x)F_1$ if $F_{2,0}$ represents the structure factor of the fully substituted material (i.e. InAs or $In_{0.53}Ga_{0.47}P$). Substituting this into eqn. (15) and calculating the intensity $I(\mathbf{K})$ gives

$$I(\mathbf{K}) = [\Phi(\mathbf{K}) + \Delta\Phi(\mathbf{K})][\Phi(\mathbf{K}) + \Delta\Phi(\mathbf{K})]^*$$

$$= \left(\frac{F_1}{A_c}\right)^2\left[\frac{\sin^2(\pi\mathbf{s} \cdot \mathbf{c}N_0)}{\sin^2(\pi\mathbf{s} \cdot \mathbf{c})} + \left(\frac{F_{2,0}}{F_1} - 1\right)^2(xN_2)^2\right.$$

$$\left. + 2\frac{\sin(\pi\mathbf{s} \cdot \mathbf{c}N_0)}{\sin(\pi\mathbf{s} \cdot \mathbf{c})}\left(\frac{F_{2,0}}{F_1} - 1\right)xN_2\cos\left[\pi\mathbf{s} \cdot \mathbf{c}(N_3 - N_1)\right]\right]. \tag{16}$$

If the total thickness N_0 and $N_3 - N_1$ (i.e. the position of the buried layer) are kept constant the intensity will only depend on the product xN_2.

For strain sensitive reflections (e.g. 202) $F_1 = F_3 \approx F_2$ and $\mathbf{g} \cdot \varepsilon\mathbf{c} \neq 0$. The modulation is then given by

$$\Delta\Phi(\mathbf{K}) = \frac{F_1}{A_c}\left\{\exp\left[-\pi i\mathbf{s} \cdot \mathbf{c}(2N_1 + N_2 - 1)\right]\left[-2i\sin\left(\pi\mathbf{g} \cdot \varepsilon\mathbf{c}\frac{N_2 - 1}{2}\right)N_2\right.\right.$$

$$\times\exp\left(-\pi i\mathbf{g} \cdot \varepsilon\mathbf{c}\frac{N_2 - 1}{2}\right)\right] + \exp\left[-\pi i\mathbf{s} \cdot \mathbf{c}(2N_1 + 2N_2 + N_3 - 1)\right]\left[-2i\sin(\pi\mathbf{g} \cdot \varepsilon\mathbf{c}N_2)\right.$$

$$\left.\left.\times\exp(-\pi i\mathbf{g} \cdot \varepsilon\mathbf{c}N_2)\right]\frac{\sin(\pi\mathbf{s} \cdot \mathbf{c}N_3)}{\sin(\pi\mathbf{s} \cdot \mathbf{c})}\right\}. \tag{17}$$

For small N_2, say $N_2 < 2$ the first term in the brackets is much smaller than the second and can be neglected. This approximation is similar to the treatment of a crystal defect, in which the exact strain profile within the fault is neglected and only the shift of the following layer due to this strain is included. If the buried layer thickness $N_2 = 1$, the second term becomes zero and the approximation is exact. The intensity is given by

$$I(\mathbf{K}) = \left(\frac{F_1}{A_c}\right)^2\left\{\frac{\sin(\pi\mathbf{s} \cdot \mathbf{c}N_0)}{\sin^2(\pi\mathbf{s} \cdot \mathbf{c})} + 4\frac{\sin^2(\pi\mathbf{g} \cdot \varepsilon\mathbf{c}N_2)\sin^2(\pi\mathbf{s} \cdot \mathbf{c}N_3)}{\sin^2(\pi\mathbf{s} \cdot \mathbf{c})}\right.$$

$$+ 4\frac{\sin(\pi\mathbf{s} \cdot \mathbf{c}N_0)\sin(\pi\mathbf{g} \cdot \varepsilon\mathbf{c}N_2)\sin(\pi\mathbf{s} \cdot \mathbf{c}N_3)}{\sin^2(\pi\mathbf{s} \cdot \mathbf{c})}$$

$$\left.\times\sin\left[\pi\mathbf{s} \cdot \mathbf{c}(N_0 - N_3) + \pi\mathbf{g} \cdot \varepsilon\mathbf{c}N_2\right]\right\}. \tag{18}$$

If N_0 and N_3 are kept constant the modulation only depends on the product εN_2.

References

BUFFAT, P. A., GANIÈRE, J. D., and STADELMANN, P., 1989, *Evaluation of Advanced Semiconductor Materials by Electron Microscopy*, edited by D. Cherns, NATO ASI Series B, Physics, 203, 319.

CHERNS, D., 1989, *Evaluation of Advanced Semiconductor Materials by Electron Microscopy*, edited by D. Cherns, NATO ASI Series B, Physics, 203, 59; 1991, *Inst. Phys. Conf. Ser.*, 117, 549.

CHERNS, D., JORDAN, I. K., and VINCENT, R., 1988a, *Phil. Mag. Lett.*, **58**, 45.

CHERNS, D., KIELY, C. J., and PRESTON, A. R., 1988b, *Ultramicroscopy*, **24**, 37.

CHERNS, D., and PRESTON, A. R., 1989, *J. Electron Microsc. Tech.*, **13**, 111.

CHERNS, D., TOUAITIA, R., PRESTON, A. R., ROSSOUW, C. J., and HOUGHTON, D. C., 1991, *Phil. Mag.*, **64**, 597.

FEWSTER, P. F., 1988, *J. appl. Crystallogr.*, **21**, 524.

HIRSCH, P. B., HOWIE, A., NICHOLSON, R. B., PASHLEY, D. W., and WHELAN, M. J., 1965, *Electron Microscopy of Thin Crystals* (London: Butterworths).

JORDAN, I. K., CHERNS, D., HOCKLY, M., and SPURDENS, P. C., 1989, *Inst. Phys. Conf. Ser.*, 100, 293.

JORDAN, I. K., GRIGORIEFF, N., CHERNS, D., HOCKLY, M., SPURDENS, P. C., AYLETT, M. R., and SCOTT, E. G., 1991b, *Inst. Phys. Conf. Ser.*, 117, 563.

JORDAN, I. K., ROSSOUW, C. J., and VINCENT, R., 1991a, *Ultramicroscopy*, **35**, 237.

VINCENT, R., 1989, *J. Electron Microsc. Tech.*, **13**, 40.